PIER M

A Triple Phase Shift Control Method for Bidirectional Inductive Power Transfer (BIPT) Systems with Fully-Compensated Series-Series (SS) Topology

Liujie Wan[1,2], Xiaohe Zhao[1,2,*], Jingkui Mao[1], and Xiu Zheng[1]

[1] *Henan Institute of Technology, Xinxiang 453000, Henan, China*
[2] *Henan Key Laboratory of Cable Structure and Materials, Xinxiang 453000, Henan, China*

ABSTRACT: A bidirectional inductive power transfer (BIPT) system of full-compensated series-series (SS) topology with full bridge converters on both primary and secondary sides is analyzed in this paper. The steady-state electrical characteristics of the BIPT system under triple-phase-shift control are obtained, based on which, the conditions for achieving the maximum transfer efficiency of the intermediate circuit and zero voltage switching of all switches are derived. Triple Phase-Shift Control (TPSC) strategy was proposed for the control of the two inner phase shifted of the primary and secondary side full bridge converters and the fundamental excitation voltage phase shift, which achieved the maximum transfer efficiency of the intermediate circuit and zero voltage switching of all switches. The proposed control method was verified through simulation. The results showed that the control strategy can realize the bidirectional energy transfer of the IPT system, the efficiency optimization of the intermediate link, and the zero-voltage turn-on of all switching devices under various load conditions.

1. INTRODUCTION

With the introduction of Energy Internet and the development of related technologies of intelligent distribution network, the bidirectional induction power transmission system (BIPT) of electric vehicles has gradually begun to show its unique advantages. For power grid, BIPT system enables bidirectional flow of electrical energy between the grid and onboard batteries. If intelligently regulated, it can achieve optimized operation functions such as orderly charging of electric vehicles and peak shaving and valley filling of the power grid. For power users, the induction power transmission method eliminates the step of connecting or disconnecting charging cables, and there are no problems such as interface wear, poor contact, or leakage. Its operation is extremely convenient. Therefore, the technical development of BIPT plays an important role in improving the stability and intelligence of the future Energy Internet [1].

Compared to the unidirectional induction energy transmission system where power can only flow from the grid to the electric vehicle battery, in BIPT system, the diode half controlled rectifier bridge on the electric vehicle side is replaced by a full bridge converter composed of fully controlled devices, which enables bidirectional transmission of electrical energy between the onboard battery and the power grid, depending on different control methods [2]. When the full bridge converter is controlled in the inverter state, power can flow from the electric vehicle battery to the grid. When the full bridge converter is controlled in synchronous rectification state, power can flow from the grid to the electric vehicle battery. In a unidirectional IPT system, to achieve autonomous regulation of charging power on the electric vehicle side, it is often necessary to cascade a DC/DC converter between the rectifier on the receiving side and the battery [3–5]. Compared to the unidirectional IPT system using semi-controlled rectifier devices, BIPT system introduces fully controlled devices instead of uncontrolled devices, which not only makes reverse power flow possible, but also utilizes a full bridge converter composed of fully controlled devices to adjust the transmission power size, thereby eliminating the DC/DC conversion link between the rectifier and the battery in traditional unidirectional IPT systems, and reducing corresponding power losses [6, 7]. In addition, if the control method proposed in this article is adopted, the zero voltage switching (ZVS) of all switching devices can be achieved by controlling the external phase angle between the full bridge converter on the ground side and the electric vehicle side, thereby reducing switching losses, improving efficiency, and reducing electromagnetic interference (EMI) [8–10].

This article establishes a steady-state mathematical model of a fully compensated SS type topology BIPT circuit, obtains the power transmission characteristics and the conditions for achieving the highest transmission efficiency in the intermediate link, analyzes the conditions for achieving zero voltage switch(ZVS) in all switch devices, and proposes a triple phase shift control scheme that takes into account transmission efficiency, transmission power, and ZVS of switch devices, and conducts simulation verification on it.

---

* Corresponding author: Xiaohe Zhao (15893860381@163.com).
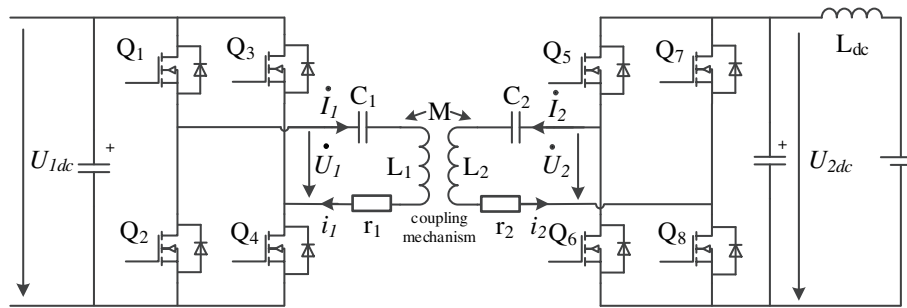
FIGURE 1. The of main circuit of the BIPT system of fully-compensated SS topology.
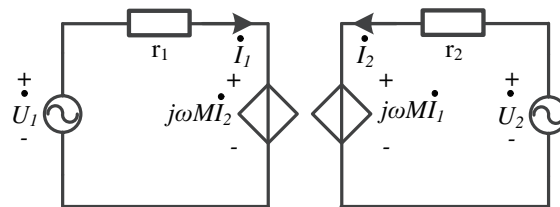
FIGURE 2. The equivalent circuit of the intermediate circuit considering only the fundamental components.

2. CHARACTERISTIC ANALYSIS OF FULLY COMPENSATED SS TOPOLOGY BIPT CIRCUIT

The common intermediate compensation topology for BIPT generally includes SS compensation, dual LCL compensation, and dual LCC compensation. Among them, the fully compensated SS topology has the fewest number of compensation components, so it has lower power loss, relatively simpler design parameters, and wider range of application prospects [11]. The main circuit of the BIPT system based on fully compensated SS topology is shown in Fig. 1, in which U_{1dc} and U_{2dc} are the DC side voltage of the primary and secondary full bridge converters (battery voltage), respectively; U_1 and U_2 are the fundamental excitation voltage outputs by the primary and secondary full bridge converters, respectively; I_1 and I_2 are the fundamental current components in the primary and secondary coils, respectively; Q_1, Q_2, Q_3, and Q_4 are the switching tubes of the full bridge converter on the original side; Q_5, Q_6, Q_7, and Q_8 are the switching tubes of the secondary side full bridge converter; C_1 and C_2 are the compensation capacitors on the primary and secondary sides, respectively; L_1 and L_2 are the self inductance of the primary and secondary sides of the coupling mechanism (coil), respectively; M is the mutual inductance coefficient between the primary and secondary coils of the coupling mechanism; L_{dc} is the secondary DC side filtering inducted used to smooth the charging or discharging current of the battery; r_1 and r_2 are equivalent resistances that represent the losses of the primary and secondary sides, respectively.

2.1. Power Transmission Characteristics of Fully Compensated SS Topology

For a fully compensated SS topology, the relationship between the capacitance values of the primary and secondary compensation capacitors and the self inductance values of the primary

and secondary coils of the coupling mechanism is as follows.

$$
\begin{cases}
L_1 C_1 = \dfrac{1}{\omega_0^2} = \dfrac{1}{(2\pi f_0)^2} \\
L_2 C_2 = \dfrac{1}{\omega_0^2} = \dfrac{1}{(2\pi f_0)^2}
\end{cases}
\tag{1}
$$

where ω_0 and f_0 are the switching angular frequency and switching frequency of the BIPT system, respectively. When the circuit parameters satisfy the above relationship, the inductances of L_1 and L_2 are completely offset by the capacitances of C_1 and C_2, respectively. Meanwhile, due to the strong bandpass filtering characteristics of the intermediate resonant link, harmonic components higher than the resonant frequency f_0 are largely filtered out. For the convenience of analysis, the fundamental analysis method can be used, considering only the fundamental component with frequency f_0 [1]. The equivalent circuit of the intermediate link in Fig. 1 is shown in Fig. 2.

This article proposes that the primary and secondary side converters of the BIPT system adopt triple phase shifting control. Let the internal displacement phase angle of the entire bridge on the original side be β_1. The internal displacement phase angle of the secondary side full bridge is $\beta_2, 0 \leq \beta_1$, $\beta_2 \leq \pi/2$; the phase difference between the fundamental voltage outputs from both full bridges is δ (The excitation voltage on the secondary side leads the excitation voltage on the primary side as positive, $-\pi/2 \leq \delta \leq \pi/2$), then the excitation voltage waveform of the full bridge output in the primary and secondary side are shown in Fig. 3, respectively.

The excitation voltage in both sides of the full bridge can be concluded by performing Fourier decomposition on the excita-
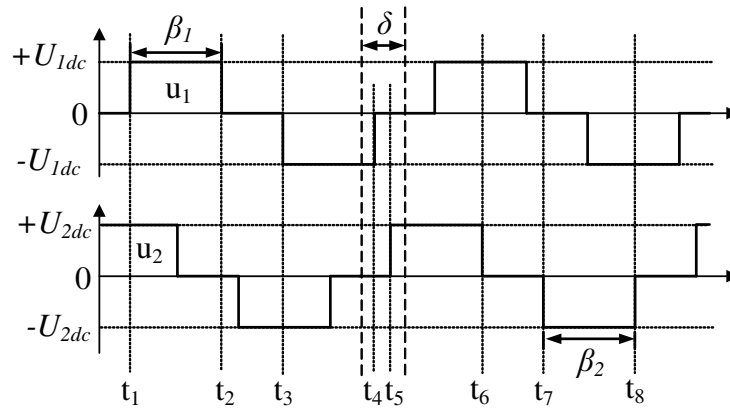
FIGURE 3. The excitation voltage of the primary and the secondary side.

tion voltage waveform.

$$\begin{cases} \left| \dot{U}_1 \right| = \dfrac{4U_{1dc}}{\sqrt{2}\pi} \sin\left(\dfrac{\beta_1}{2}\right) \\[3mm] \left| \dot{U}_2 \right| = \dfrac{4U_{2dc}}{\sqrt{2}\pi} \sin\left(\dfrac{\beta_2}{2}\right) \end{cases} \tag{2}$$

Due to the relatively small equivalent resistances of r_1 and r_2, the voltage drop on them can be ignored, and the fundamental current phase on the both sides can be obtained.

$$\begin{cases} \dot{I}_1 = -\dfrac{j}{\omega_0 M}\dot{U}_2 \\[3mm] \dot{I}_2 = -\dfrac{j}{\omega_0 M}\dot{U}_1 \end{cases} \tag{3}$$

When the power flows from the primary side (ground charging station) to the secondary side (electric vehicle) in the positive direction, the transmission power when ignoring losses is shown as below.

$$P = Re\left(\dot{U}_1 \dot{I}_1^*\right) = \frac{\left|\dot{U}_1\right|\left|\dot{U}_2\right| \sin\delta}{\omega_0 M}$$

$$= \frac{8U_{1dc}U_{2dc}}{\omega_0 M \pi^2} \sin\left(\frac{\beta_1}{2}\right) \sin\left(\frac{\beta_2}{2}\right) \sin\delta \tag{4}$$

From Eq. (4), it can be seen that it is a necessary condition of maintaining the fundamental phase difference δ of the excitation voltage for maintaining a constant direction and magnitude of power transmission. The adjustment of transmission power size and direction can be achieved by adjusting the β_1, β_2, δ control implementation.

2.2. Analysis of the Highest Transmission Efficiency of Intermediate Links

To analyze the highest transmission efficiency, it is necessary to consider the losses on equivalent resistors r_1 and r_2. According

to Fig. 2, the total losses on r_1 and r_2 can be solved.

$$P_{loss} = \left|\dot{I}_1\right|^2 r_1 + \left|\dot{I}_2\right|^2 r_2 = \frac{\left|\dot{U}_1\right|^2 r_2 + \left|\dot{U}_2\right|^2 r_1}{M^2\omega_0^2 + r_1 r_2} \tag{5}$$

Taking the flow of power from the primary side to the secondary side as an example, the input power of the excitation voltage port on the primary side is as follows.

$$P_{input} = \mathrm{Re}\left(\dot{U}_1 \dot{I}_1^*\right) = \frac{\left(M\sin(\delta)\omega_0 \left|\dot{U}_2\right| + \left|\dot{U}_1\right| r_2\right)\left|\dot{U}_1\right|}{M^2\omega_0^2 + r_1 r_2} \tag{6}$$

The transmission efficiency of the intermediate link can be obtained as follows.

$$\eta = \frac{P_{input} - P_{loss}}{P_{input}} = \frac{\left|\dot{U}_2\right|\left(M\sin(\delta)\omega_0\left|\dot{U}_1\right| - \left|\dot{U}_2\right| r_1\right)}{\left|\dot{U}_1\right|\left(M\sin(\delta)\omega_0\left|\dot{U}_2\right| + \left|\dot{U}_1\right| r_2\right)}$$

$$= 1 - \frac{\kappa^2 r_2 + \chi r_2}{M\sin(\delta)\omega_0\kappa + \kappa^2 r_2} \tag{7}$$

where

$$\begin{cases} \kappa = \dfrac{\left|\dot{U}_1\right|}{\left|\dot{U}_2\right|} \\[3mm] \chi = \dfrac{r_1}{r_2} \end{cases} \tag{8}$$

When the transmission efficiency of the intermediate link is maximized, the voltage ratio between the primary and secondary sides is as follows.

$$\frac{\left|\dot{U}_1\right|}{\left|\dot{U}_2\right|} = \kappa = \frac{\chi r_2 + \sqrt{\chi^2 r_2^2 + M^2 \sin^2(\delta)\omega_0^2\chi}}{M\sin(\delta)\omega_0} = \kappa_{opt} \tag{9}$$

When the power flows from the secondary side to the primary side, a similar conclusion can also be drawn. In practical

situations, the following relationship is generally satisfied by the following equation.

$$\chi r_2 \ll M \sin(\delta) \omega_0 \sqrt{\chi}$$

$$\chi^2 r_2^2 \ll M^2 \sin^2(\delta) \omega_0^2 \chi \tag{10}$$

Therefore, in order to achieve the highest transmission efficiency, the conditions that need to be met can be approximately simplified as follows.

$$\frac{\left|\dot{U}_1\right|}{\left|\dot{U}_2\right|} = \frac{U_{1dc}\sin\left(\frac{\beta_1}{2}\right)}{U_{2dc}\sin\left(\frac{\beta_2}{2}\right)} = \kappa_{opt} = \frac{|\dot{I}_2|}{|\dot{I}_1|} \approx \sqrt{\chi} = \sqrt{\frac{r_1}{r_2}} \tag{11}$$

This condition can be qualitatively explained as follows: when the above conditions are met, the power losses on the equivalent loss resistors r_1 and r_2 are approximately equal, and the total power loss is the lowest. At this point, the transmission efficiency of the intermediate link reaches the highest. In the actual process, the transmission efficiency of the intermediate link can be optimized by controlling the internal phase shift angles β_1 and β_2 of the primary and secondary sides.

2.3. Analysis of Zero Voltage Turn-on Conditions for Switching Devices

For converters with high switching frequency and power level, zero voltage switch (ZVS) for switching devices is an important condition for reducing switch losses and electromagnetic interference. Due to the use of semi-controlled rectification on the secondary side, the fundamental phase of the voltage on the AC side of the rectifier bridge is approximately the same as the fundamental phase of the current on the secondary side, i.e., $|\delta| \approx 90°$. If the primary side full bridge converter adopts internal phase shifting for power regulation, the range of ZVS achieved by the primary side full bridge switching transistor is extremely narrow, and ZVS cannot be achieved in most operating conditions. For the BIPT system in this article, due to the use of fully controlled devices in the AC/DC converter on the secondary side, it can be achieved by adjusting the δ value adjustment to achieve ZVS.

Taking the power flowing from the primary side to the secondary side (forward power transmission) as an example, according to the analysis in Subsection 2.1, the fundamental phase of the both side currents can be expressed as follows.

$$\begin{cases} \dot{I}_1 = \frac{4U_{2dc}}{\omega M \pi} \sin\left(\frac{\beta_2}{2}\right)(\sin\delta - j\cos\delta) \\ \dot{I}_2 = -\frac{j}{\omega M} \frac{4U_{1dc}}{\pi} \sin\left(\frac{\beta_1}{2}\right) \end{cases} \tag{12}$$

The time-domain form is as follows.

$$\begin{cases} i_1(t) = -\frac{4U_{dc2}}{\omega M \pi} \sin\left(\frac{\beta_2}{2}\right) \cos(\omega t + \delta) \\ i_2(t) = -\frac{4U_{dc1}}{\omega M \pi} \sin\left(\frac{\beta_1}{2}\right) \cos(\omega t) \end{cases} \tag{13}$$

The drive-time relationship of the switching tubes on the both sides is shown in Fig. 4. The driving signals of the upper and lower tubes on each bridge arm are complementary and have a certain dead zone. For a certain switching tube, if its antiparallel diode conducts before the switching tube, its terminal voltage can be clamped to zero by the conducting diode before the switching tube conducts, and the switching tube can achieve zero voltage turn-on. In order to analyze conveniently, ignoring the junction capacitance between MOSFET DS switches, it can be concluded that the conditions for achieving ZVS are as follows, based on the above considerations,

$$\begin{cases} i_1(t_1) < 0 \\ i_1(t_2) > 0 \\ i_1(t_3) > 0 \\ i_1(t_4) < 0 \\ i_2(t_5) < 0 \\ i_2(t_6) > 0 \\ i_2(t_7) > 0 \\ i_2(t_8) < 0 \end{cases} \text{among which:} \begin{cases} t_1 = \frac{1}{2}\frac{\pi - \beta_1}{\omega_0} \\ t_2 = \frac{1}{2}\frac{\pi + \beta_1}{\omega_0} \\ t_3 = \frac{1}{2}\frac{3\pi - \beta_1}{\omega_0} \\ t_4 = \frac{1}{2}\frac{3\pi + \beta_1}{\omega_0} \\ t_5 = \frac{1}{2}\frac{\pi - \beta_2 - 2\delta}{\omega_0} \\ t_6 = \frac{1}{2}\frac{\pi + \beta_2 - 2\delta}{\omega_0} \\ t_7 = \frac{1}{2}\frac{3\pi - \beta_2 - 2\delta}{\omega_0} \\ t_8 = \frac{1}{2}\frac{3\pi + \beta_2 - 2\delta}{\omega_0} \end{cases} \tag{14}$$

According to the symmetry of the current waveform in the positive and negative half cycles, the above formula can be simplified as follows.

$$\begin{cases} i_1(t_1) < 0 \\ i_1(t_2) > 0 \\ i_2(t_5) < 0 \\ i_2(t_6) > 0 \end{cases}, \text{ it is:} \begin{cases} \sin\left(-\frac{1}{2}\beta_1 + \delta\right) < 0 \\ \sin\left(\frac{1}{2}\beta_1 + \delta\right) > 0 \\ \sin\left(\frac{1}{2}\beta_2 + \delta\right) > 0 \\ \sin\left(-\frac{1}{2}\beta_2 + \delta\right) < 0 \end{cases} \tag{15}$$

According to the range of β_1, β_2, and δ, the conditions for achieving ZVS of all switching devices are as follows.

$$\begin{cases} |\delta| < \frac{\beta_1}{2} \\ |\delta| < \frac{\beta_2}{2} \end{cases} \tag{16}$$
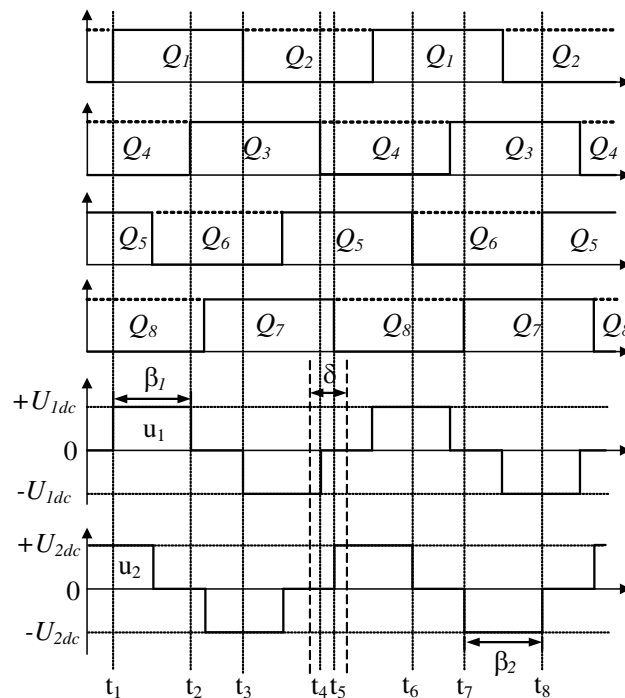
FIGURE 4. The driving signal of switching components and the waveform of the formed excitation voltage.

That is to say, without considering the junction capacitance of the switching transistor, in order to achieve ZVS, it is necessary to ensure that the absolute value of the fundamental phase difference of the excitation voltage on both sides is less than half of the minimum internal phase angle value in the two side converters. In practice, considering the influence of switch junction capacitance, a certain margin needs to be left to make the absolute value of the fundamental phase difference slightly smaller than the critical value.

$$|\delta| = \frac{\min\{\beta_1, \beta_2\}}{2} - \alpha, \quad \alpha > 0 \qquad (17)$$

3. IMPLEMENTATION OF TRIPLE PHASE SHIFT CONTROL STRATEGY

The BIPT system needs to control the charging/discharging power of electric vehicle batteries, while also taking into account overall efficiency and finding ways to reduce external electromagnetic interference. According to the previous content, the control method proposed in this article has three degrees of freedom, namely the internal phase shift angle of the primary side full bridge converter β_1, the internal phase shift angle of the secondary side full bridge converter β_2, and the fundamental phase difference of the primary and secondary side excitation voltage δ. According to the previous conclusion, the transmission power is influenced by three controlled variables. The fundamental amplitude of the excitation voltage on the primary and secondary sides depends on the internal phase shift angle of the full bridge converter of the corresponding side. The fundamental power factor of the AC port of the bilateral

converter is determined by the fundamental phase difference. From the analysis in Subsection 2.3, it can be concluded that in order to achieve ZVS for all switching devices, it is necessary to make the value of $|\delta|$ not equal to 90°. However, according to the expression of transmission power, compared to the case where $|\delta| = 90°$, when $|\delta|$ is not equal to 90°, a higher value of β_1 or β_2 is required to achieve the same transmission power. According to the conclusion in Subsection 2.2, in order to achieve the highest transmission efficiency in the intermediate link, it is necessary to increase β_1 and β_2 simultaneously, which leads to an increase in the RMS value of the fundamental wave of the excitation voltage on both sides, resulting in an increase in the RMS of the resonant current in the primary and secondary loops. As a result, higher losses will be generated at the equivalent resistors r_1 and r_2. To avoid additional losses on r_1 and r_2, it is necessary to maintain $|\delta| = 90°$, but at this point, some switching devices will be in a hard open state, which increases its losses. If low-cost silicon material switching tubes are used, the losses caused by hard switching of the switching device will be higher than the additional losses generated on r_1 and r_2 when A deviates from B under the same transmission power. Therefore, priority should be given to ensuring that all switch tubes achieve ZVS.

Based on the above control requirements, this article develops a control strategy for the BIPT system as shown in Fig. 5. In this system, the secondary side battery has two control modes: constant voltage mode and constant current mode. The constant current mode is used to control the charging or discharging current of the battery to a given value, while the constant voltage mode is generally used during the constant voltage charging stage of the battery. The control of charging and discharging
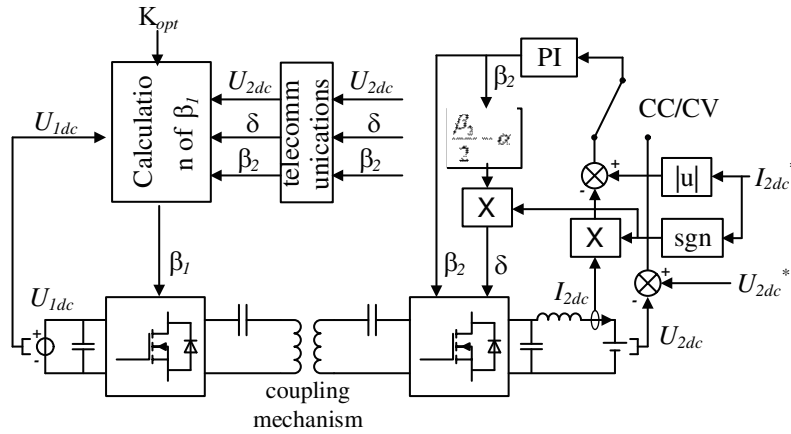
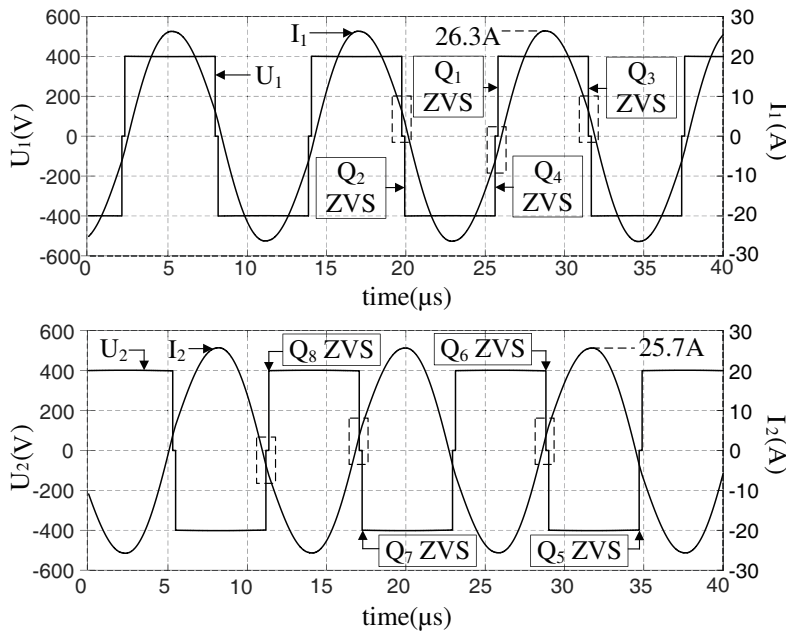FIGURE 5. The proposed control method.

FIGURE 6. Forward power flow, full load, $\beta_1 = \beta_2 = 174°$, $\delta = 82°$.

current or battery voltage is essentially the control of transmission power.

As shown in Fig. 5, first of all, calculate the error between the battery current or voltage and the corresponding given value, and send it to the proportional integral (PI) regulator for operation to obtain the internal displacement phase angle value β_2 of the full bridge in secondary side. Then, according to the ZVS condition in Subsection 2.3, calculate the fundamental phase difference δ, and send it to the PWM modulation stage to drive the full bridge converter in the secondary side. At the same time, send the secondary side information to the primary side controller through wireless communication. Finally, the primary controller calculates the internal phase angle of the primary full bridge converter according to Eq. (18) and sends it to the modulation stage of the primary full bridge converter.

$$\beta_1 = \max\left\{ 2\sin^{-1}\left(\frac{\kappa_{opt} U_{2dc}}{U_{1dc}} \sin\left(\frac{\beta_2}{2}\right) \right), 2\left(|\delta| + \alpha\right) \right\} \quad (18)$$

From Eq. (18), it can be seen that the proposed control method prioritizes the implementation of switching tube ZVS and secondly strives to make the ratio of excitation voltages on the primary and secondary sides equal to the optimal ratio as much as possible to optimize the transmission efficiency of intermediate links.

4. SIMULATION VERIFICATION

To verify the correctness of the control method proposed in this article, simulation validation was conducted on the CloudPSS cloud simulation platform. The BIPT system parameters in the simulation are shown in Table 1, and the coupling mechanism parameters are taken from the parameters of an actual coupling mechanism. When the primary and secondary coil structures of the coupling mechanism are symmetrical, the primary and
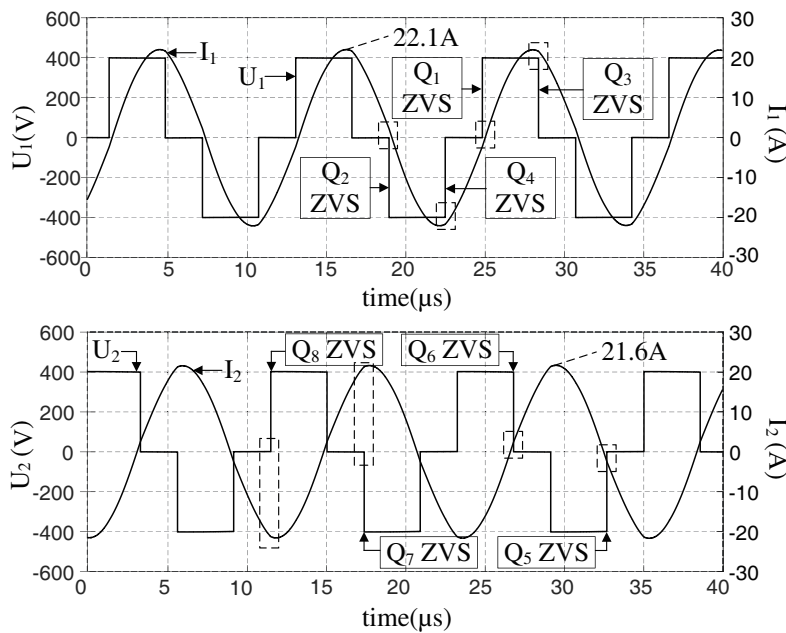
FIGURE 7. Forward power flow, half load, $\beta_1 = \beta_2 = 108°$, $\delta = 49°$.

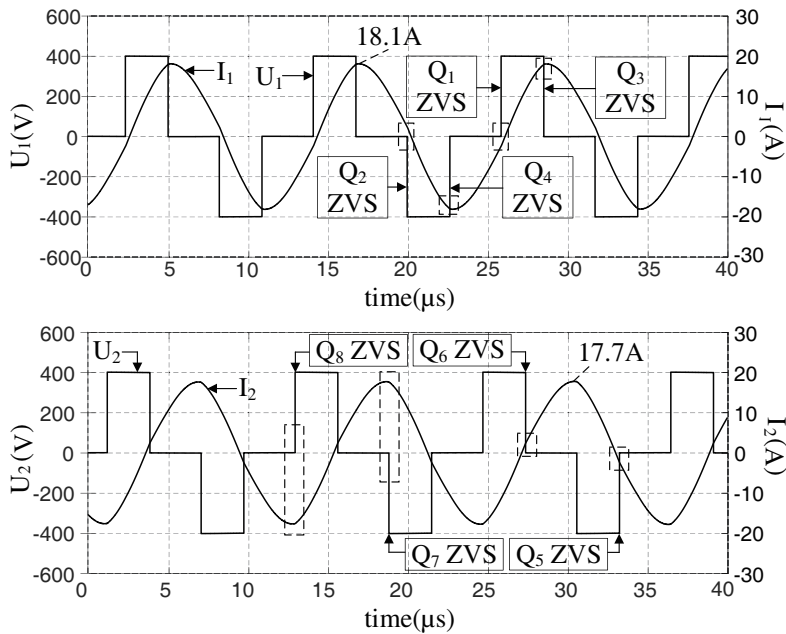**FIGURE 8**. Forward power flow, 1/4 load, $\beta_1 = \beta_2 = 82°$, $\delta = 36°$.

secondary sides have the same impedance coefficient, $r_1 = r_2$, $K_{opt} \approx 1$.

Given the transmission power of 6.6 kW (full load), 3.3 kW (half load), 1.65 kW (1/4 load) respectively in the forward direction, and 6.6 kW (full load) in the reverse direction, simulation was conducted on the CloudPSS cloud platform using the control method described in Section 3. The simulation results are shown in Figs. 6 to 9, respectively. By analyzing the phase relationship between the excitation voltages of the primary and secondary sides and their respective currents in each figure, it can be concluded that for Fig. 6 to Fig. 8, the absolute value of

the phase difference between the fundamental waves of U_1 and I_1 is less than 90°, indicating the power output from the ports. The absolute value of the phase difference between the fundamental waves of U_2 and I_2 is greater than 90°, and the port absorbs power. For Fig. 9, the absolute value of the phase difference between the fundamental waves of U_1 and I_1 is greater than 90°, and the port absorbs power. The absolute value of the phase difference between the fundamental waves of U_2 and I_2 is less than 90°, and the port emits power. For Fig. 9, power is transmitted from the secondary side to the primary side. In

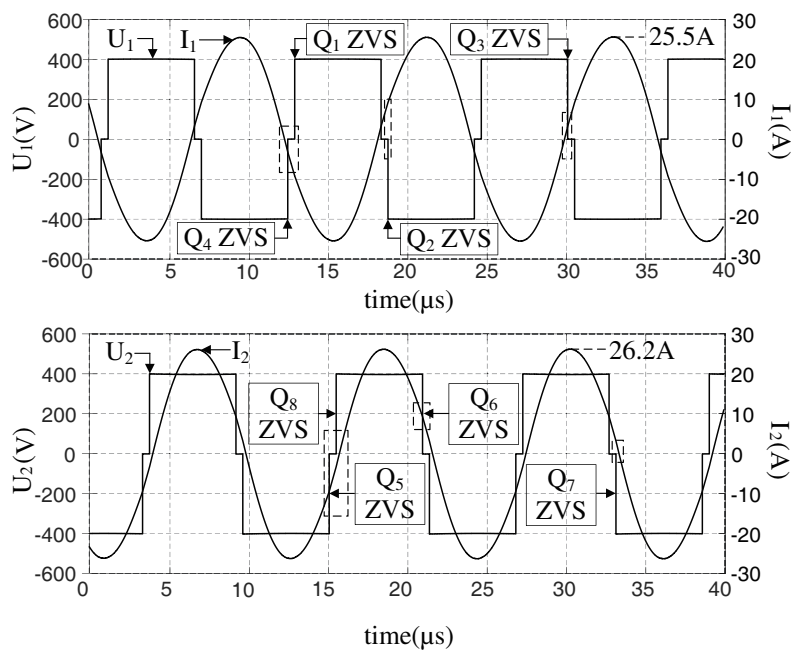**FIGURE 9**. Backward power flow, full load, $\beta_1 = \beta_2 = 167°$, $\delta = -78°$.

TABLE 1. Parameters of the BIPT system.

Circuit parameter	value	Circuit parameter	value
U_{1dc}	400 V	C_1	19.796 nF
U_{2dc}	400 V	C_2	19.83 nF
P_N	6.6 kW	r_1	161 mΩ
L_1	177.1 µH	r_2	161 mΩ
L_2	176.8 µH	f	85 kHz
M	36 µH	α	5°

summary, the system has achieved bidirectional energy transmission.

Based on the conclusion in Subsection 2.2 and the parameters given in Table 1, it can be concluded that when the transmission efficiency of the intermediate link reaches its maximum, the ratio of the amplitude of the primary and secondary currents should be approximately equal to 1. According to Figs. 6 to 9, under four different operating conditions, the ratio of primary and secondary currents is 1.0233, 1.0231, 1.0226, and 0.9733, respectively. The ratio of primary and secondary currents is close to 1, which meets the conditions for achieving the highest transmission efficiency in the intermediate link and optimizes the transmission efficiency of the intermediate link.

According to the conclusion in Subsection 2.3, in order to achieve zero voltage turn-on of all switching devices, the antiparallel diode of the switching transistor must conduct before the switching transistor. To achieve this condition, at the moment before Q_1, Q_2, Q_3, and Q_4 conduct, the primary current i_1 should be negative, positive, positive, and negative, respectively, according to the reference direction in Fig. 1. At the moment before conducting in Q_5, Q_6, Q_7, and Q_8, the secondary current I_2 should be negative, positive, positive, and negative,

respectively. From Figs. 6 to 9, the above zero voltage turn-on conditions are met, and all switching devices can achieve ZVS.

5. CONCLUSION

This article establishes a steady-state mathematical model of a BIPT system with a full bridge converter for the primary and secondary sides, and a fully compensated SS topology for the intermediate link. The power transmission characteristics, conditions for achieving the highest transmission efficiency in the intermediate link, and conditions for achieving zero voltage turn-on of all switching devices are analyzed. A triple phase shift control scheme is proposed, which utilizes the internal phase shift angle of the primary and secondary full bridge converters and the fundamental phase difference of the excitation voltage of the primary and secondary sides as three control variables to achieve bidirectional energy transmission, optimization of intermediate link transmission efficiency, and zero voltage turn-on of all switching devices over a wide load range. Finally, the correctness of the proposed control method is verified by establishing a simulation model on the CloudPSS cloud simulation platform.

REFERENCES

[1] Chen, K., Z. Zhao, L. Fang, *et al.*, "Analysis of resonant topology for bi-directional wireless charging of electric vehicle," *Automation of Electric Power Systems*, 2017.

[2] Li, Y., Y. Sun, X. Dai, and J. Zhou, "Modeling and control of an LCL bi-directional inductive power transfer system," *Journal of Chongqing University*, Vol. 35, No. 10, 117–123, 2012.

[3] Bosshard, R. and J. W. Kolar, "All-SiC 9.5 kW/dm^3 on-board power electronics for 50 kW/85 kHz automotive IPT system," *IEEE Journal of Emerging and Selected Topics in Power Electronics*, Vol. 5, No. 1, 419–431, 2017.

[4] Ishihara, H., F. Moritsuka, H. Kudo, S. Obayashi, T. Itakura, A. Matsushita, H. Mochikawa, and S. Otaka, "A voltage ratio-based efficiency control method for 3 kW wireless power transmission," in *2014 IEEE Applied Power Electronics Conference and Exposition — APEC 2014*, 1312–1316, IEEE, 2014.

[5] Hata, K., T. Imura, and Y. Hori, "Dynamic wireless power transfer system for electric vehicles to simplify ground facilities-power control and efficiency maximization on the secondary side," in *2016 IEEE Applied Power Electronics Conference and Exposition (APEC)*, 1731–1736, IEEE, 2016.

[6] Nguyen, B. X., D. M. Vilathgamuwa, G. H. B. Foo, P. Wang, A. Ong, U. K. Madawala, and T. D. Nguyen, "An efficiency optimization scheme for bidirectional inductive power transfer systems," *IEEE Transactions on Power Electronics*, Vol. 30, No. 11, 6310–6319, 2015.

[7] Diekhans, T. and R. W. D. Doncker, "A dual-side controlled inductive power transfer system optimized for large coupling factor variations and partial load," *IEEE Transactions on Power Electronics*, Vol. 30, No. 11, 6320–6328, 2015.

[8] Madawala, U. K. and D. J. Thrimawithana, "A bidirectional inductive power interface for electric vehicles in V2G systems," *IEEE Transactions on Industrial Electronics*, Vol. 58, No. 10, 4789–4796, 2011.

[9] Zhou, L. and J. Jiang, "Analysis and control of dual active bridge DC-DC converter based on LCL resonant network," *Automation of Electric Power Systems*, Vol. 40, No. 19, 82–86, 2016.

[10] Li, S., W. Li, J. Deng, T. D. Nguyen, and C. C. Mi, "A double-sided LCC compensation network and its tuning method for wireless power transfer," *IEEE Transactions on Vehicular Technology*, Vol. 64, No. 6, 2261–2273, 2015.

[11] Liu, C., Y. Guo, S. Ge, G. Cai, and F. Zhou, "Characteristics analysis and experimental verification of the double LCL resonant compensation network for electrical vehicles wireless power transfer," *Transactions of China Electrotechnical Society*, Vol. 30, No. 15, 127–135, 2015.